OPEN

Correspondence and requests for materials should be addressed to A.O. (ozcan@ucla. edu) or H.A. (hatice. altug@epfl.ch)

* These authors contributed equally to this work.

Lensfree optofluidic plasmonic sensor for real-time and label-free monitoring of molecular binding events over a wide field-of-view

Ahmet F. Coskun[1,3]*, Arif E. Cetin[2,5]*, Betty C. Galarreta[2,4]*, Daniel Adrianzen Alvarez[2], Hatice Altug[2,5] & Aydogan Ozcan[1,6]

[1]Departments of Electrical Engineering and Bioengineering, University of California, Los Angeles (UCLA), CA 90095, USA, [2]Department of Electrical and Computer Engineering, Boston University, MA 02215, USA, [3]Division of Chemistry and Chemical Engineering, California Institute of Technology, Pasadena, CA, 91125, [4]Pontificia Universidad Catolica del Peru, Departamento de Ciencias-Quimica, Avenida Universitaria 1801, Lima 32, Peru, [5]Bioengineering Department, Ecole Polytechnique Federale de Lausanne (EPFL), Lausanne CH-1015 Switzerland, [6]California NanoSystems Institute, University of California, Los Angeles (UCLA), CA 90095, USA.

We demonstrate a high-throughput biosensing device that utilizes microfluidics based plasmonic microarrays incorporated with dual-color on-chip imaging toward real-time and label-free monitoring of biomolecular interactions over a wide field-of-view of >20 mm². Weighing 40 grams with 8.8 cm in height, this biosensor utilizes an opto-electronic imager chip to record the diffraction patterns of plasmonic nanoapertures embedded within microfluidic channels, enabling real-time analyte exchange. This plasmonic chip is simultaneously illuminated by two different light-emitting-diodes that are spectrally located at the right and left sides of the plasmonic resonance mode, yielding two different diffraction patterns for each nanoaperture array. Refractive index changes of the medium surrounding the near-field of the nanostructures, e.g., due to molecular binding events, induce a frequency shift in the plasmonic modes of the nanoaperture array, causing a signal enhancement in one of the diffraction patterns while suppressing the other. Based on ratiometric analysis of these diffraction images acquired at the detector-array, we demonstrate the proof-of-concept of this biosensor by monitoring in real-time biomolecular interactions of protein A/G with immunoglobulin G (IgG) antibody. For high-throughput on-chip fabrication of these biosensors, we also introduce a deep ultra-violet lithography technique to simultaneously pattern thousands of plasmonic arrays in a cost-effective manner.

Compact and light-weight diagnostic devices hold significant promise for early detection and monitoring of diseases in field settings. Such point of care tools[1] aim to replace bulky equipment that are frequently used in medical labs, which can potentially enable decentralized biomedical testing and diagnosis in both developed and developing parts of the world. These field-deployable devices can be used as optical biosensors[2–4] through labelling methods or label-free techniques to detect e.g., nucleic acids, proteins and pathogens in field conditions. For instance, fluorescence labelling has been widely employed as a read-out mechanism in various biochemical assays; however, the intricate sample preparation procedures pose certain challenges on field use of such fluorescence based diagnostic technologies. Therefore, label-free detection approaches[5] provide simple and rapid biosensing devices that can be used for sensitive and specific detection of biomolecular interactions. These label-free platforms should ideally be able to monitor multiple biomarkers simultaneously for accurate diagnosis of diseases, which necessitates high-throughput screening techniques. Towards this end, there has been considerable effort to develop high-throughput label-free sensors utilizing surface plasmon resonance (SPR)[6], photonic crystals[7], optical micro-cavities[8], interferometry[9], as well as nanostructured metal substrates, e.g., subwavelength nanohole arrays[10], among others. Despite their high performance sensing and biodetection potential, most of these techniques are based on benchtop instruments, which constrains their use in remote and field settings. Thus, there is an emerging need to devise field-portable forms of these biosensors to achieve high-throughput detection without the use of any labels[11]. Along these lines, we have recently introduced a handheld plasmonic

biosensing device[12] that merges on-chip imaging and nanohole arrays towards detection of ultrathin protein layers, which might find use in field deployable sensing applications.

In this work, as an improved solution to this important need, we demonstrate a microfluidics based plasmonic biosensing system that integrates plasmonic microarrays with dual-color lensfree imaging for real-time and multiplexed monitoring of binding events over a wide field-of-view of larger than 20 mm² in low resource settings. In this platform (see Figs. 1a and 1b), we utilize an opto-electronic sensor (Complementary Metal–Oxide–Semiconductor - CMOS) to record the diffraction patterns of plasmonic nano-apertures located at the bottom of a microfluidic channel (see the photograph in Fig. 1c), enabling controlled delivery of target solution to the surface functionalized nanosensor arrays (see the Methods section for dual-color lensfree imaging set-up). As illustrated in Fig. 1d, the target proteins are captured on the plasmonic pixels that are functionalized by the ligand proteins. In our biosensing platform, the use of a plasmonic nanohole array provides high sensitivities to surface conditions due to the strong light confinements and high field enhancements at nanoscale[13–15]. Changes in the refractive index within the proximity of the sensor surface induce a spectral shift in the peak wavelength of the plasmonic mode supported by the nanohole array. We have recently investigated the use of such nanohole arrays for biosensing applications including detection of proteins and infectious viruses from biological media[14,15]. The shift in the peak wavelength of the plasmonic mode can also be determined over large areas using a CMOS or a CCD (Charge-Coupled Device) based imager[16] when the nanostructures are excited using an illumination source, e.g., a light emitting diode (LED) with a spectrum tuned to the plasmonic mode of the nanohole array.

Compared to spectrometer-based analysis of plasmonic substrates, the use of a lensfree on-chip imager as a biosensing approach to probe the plasmonic mode offers higher multiplexing capability, where multiple plasmonic nanostructures can be analysed simultaneously rather than measuring each plasmonic structure sequentially. The *merge* of microfluidics[17] with plasmonic detection and lensfree imaging also provides various advantages: (*i*) The sample preparation (collection and processing of target analytes) can be integrated with the plasmonic detection on the same platform, creating an automated biosensing tool for field use. (*ii*) The precise delivery of analytes to the plasmonic substrate improves the sensitivity and detection limit of the plasmonic biosensor. (*iii*) The ability to deliver the sample onto the plasmonic substrate over time allows rapid monitoring of binding events without the need for any labels. (*iv*) The sample exchange with fluidic injection and withdrawal also increases the multiplexing capability of the biosensing platform, where multiple analytes can be monitored over a wide range of concentrations on the same substrate (see the Methods section and Supplementary Fig. 1 for the structure of the microfluidic chamber design).

The plasmonic substrate utilized in our biosensor platform, containing arrays of plasmonic pixels, is simultaneously illuminated by two different color LEDs (Fig. 1a inset shows the photograph of the LEDs, at 820 nm and 880 nm, respectively) tuned spectrally to the right and left sides of the plasmonic mode (see Fig. 2a). The two resulting diffraction patterns for each plasmonic pixel are recorded by the CMOS detector as schematically illustrated in Fig. 2c. For our image analysis, we utilize the configuration where the center-to-center distance between two LED sources is $D = 11\ mm$ (see Supplementary Fig. 2 for diffraction pattern positions for different LED separation distances). These lensfree diffraction patterns can be numerically estimated using a spatial convolution and the Fresnel kernel approach, as detailed in our previous work[12] (also see Supplementary Fig. 3 for the details of transmission calculations for our dual LED configuration). Briefly, the local electromagnetic field distribution determined by finite difference time domain (FDTD) simulation at the plasmonic chip surface is first transformed from the spatial domain into the frequency space, next propagated over a vertical distance of 2 mm, and finally transferred back to the spatial domain to determine the diffraction pattern where the CMOS active area is present. The refractive index change of the medium covering the plasmonic nanostructures shifts the plasmonic modes such that the total transmission signal in the diffraction patterns of the nanohole arrays varies. Fig. 2b exemplifies this fact by monitoring the change in the plasmonic pixels under DI-water ($n = 1.3330$) and sucrose solution of 1.1 mol/L ($n = 1.3860$). As the refractive index of
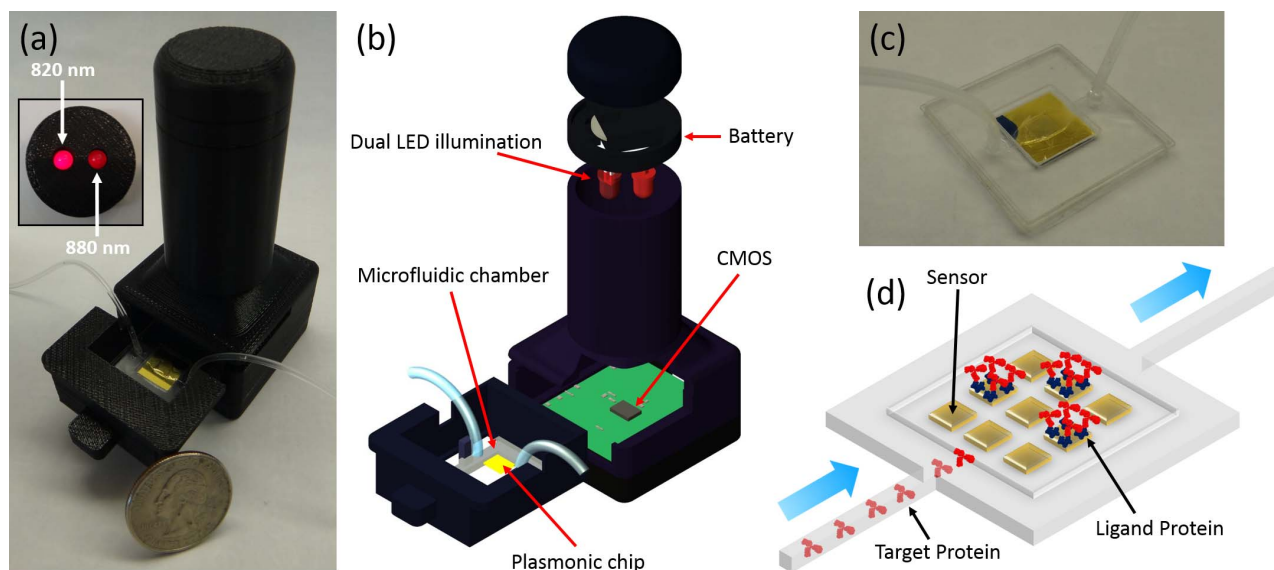

Figure 1 | **Microfluidics based high-throughput plasmonic biosensing platform using dual-color lensfree on-chip imaging configuration.** (a) Photograph of the on-chip sensing device that employs a plasmonic substrate located at the bottom of a microfluidic channel. Figure Inset: The head of the lensfree device that contains two spectrally different LEDs (with 820 nm and 880 nm peak wavelengths) for simultaneous illumination of the microfluidic chip. (b) Schematics of the on-chip biosensing device composed of a battery, two LEDs, a plasmonic chip, a microfluidic chamber, and a CMOS imager chip. (c) Photograph of the microfluidic system with inlet and outlet ports. (d) Schematic illustration of the flow-over scheme for delivery of target samples to the plasmonic substrate.
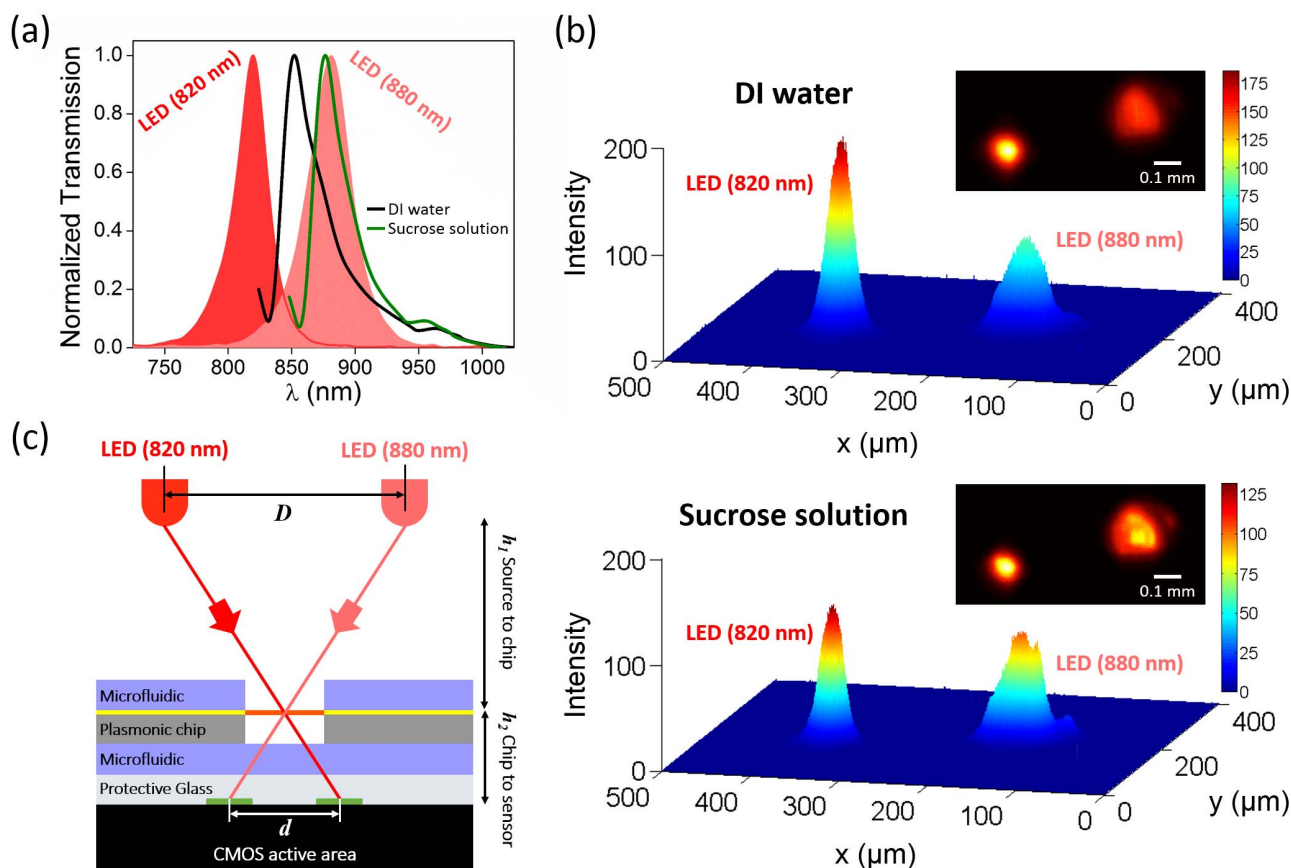
Figure 2 | Operation principles of dual-wavelength plasmonic detection platform. (a) Solid curves: Spectral variation in the plasmonic mode supported by the nanohole arrays under DI-water and sucrose solution 1.1 M. Filled curves: The spectral responses of the two LEDs employed by the lensfree on-chip imaging platform with peak wavelengths of 820 nm and 880 nm. (b) 3D visualization of the intensity of the dual diffraction pattern of the nanohole arrays formed by LED illuminations at 820 nm and 880 nm under DI-water and sucrose solution, respectively. Figure inset: Raw lensfree dual diffraction image for a single plasmonic pixel. (c) Schematic illustration of the generation of dual-diffraction patterns at the detector plane of the lensfree platform. LED separation distance: D, dual diffraction pattern separation distance: d, LED to plasmonic chip: h_1, and plasmonic chip to on-chip imager active area: h_2.

the bulk solution increases, the plasmonic mode shifts to longer wavelengths from 852 nm to 878 nm, as shown in Fig. 2a. Hence, the intensity of the diffraction pattern of the nanohole arrays formed by the LED illumination at 820 nm decreases, whereas it increases at 880 nm illumination. The ratio of these two transmitted signals obtained from one plasmonic pixel is used to increase the image contrast resulting from the spectral shift of the plasmonic mode. This ratiometric analysis that is enabled with a dual-color LED illumination configuration offers more robust and reliable spectral variation information compared to a single LED illumination[10,12] (see the Methods section).

For field-settings and point-of-care applications, it is important to reduce the cost of the consumables including the sensor chip. Toward this goal, we introduce a new fabrication method based on deep ultra-violet (UV) lithography (see Fig. 3d for the illustration of the fabrication process) that can create thousands of high fidelity plasmonic biosensor pixels at low cost, which is highly important for field applications. Compared to the fabrication of plasmonic chips using conventional Electron Beam Lithography, which is sequentially performed on each chip, we perform deep UV lithography at wafer scale within less than a minute of exposition time, followed by standard fabrication procedures (see the Methods section for the details of the fabrication method). Our fabrication method is highly flexible such that plasmonic sensor chips with different designs employing various sensor pixel numbers, sizes or spatial arrangements can be conveniently manufactured. For this work, on a 4-inch wafer (see Fig. 3a), we fabricated more than 50

plasmonic sensor chips with 1 cm × 1 cm dimension (see Fig. 3b), where each chip covers 8 square membranes/pixels with 100 μm × 100 μm dimension containing approximately 28,000 nanoapertures. Fig. 3c shows the scanning electron microscope (SEM) image of the sensor chip, demonstrating the uniformity of the nanoapertures achieved by our fabrication method.

Results and Discussion

To evaluate the sensitivity of our biosensing platform, we performed quantitative concentration experiments using sugar solutions with known refractive indices (see the Methods section for sensitivity analysis) within the microfluidic channels that uniformly cover our plasmonic substrates. The results presented in Fig. 4a demonstrate that the increase in the sucrose concentration from 0.055 to 1.1 mol/L causes the plasmonic mode to red shift, which is measured by a spectrometer for comparison purposes (see the Methods section). For this sugar concentration range, the amount of peak wavelength shift varies from 1.26 nm to 31.34 nm, which corresponds to a change in the bulk refractive index from 1.3356 to 1.3860. Fig. 4b shows the statistical analysis of this peak wavelength of the plasmonic mode supported by the nanohole array embedded in DI-water and the sucrose solutions at different concentrations. Fig. 4c demonstrates the corresponding relative intensity ratios (IRs) determined from our dual-wavelength lensfree images for each sample. These results exhibit a high correlation between the wavelength shift information (acquired by a spectrometer) and the ratiometric analysis of our dual-wavelength lensfree diffraction images. In the lens-
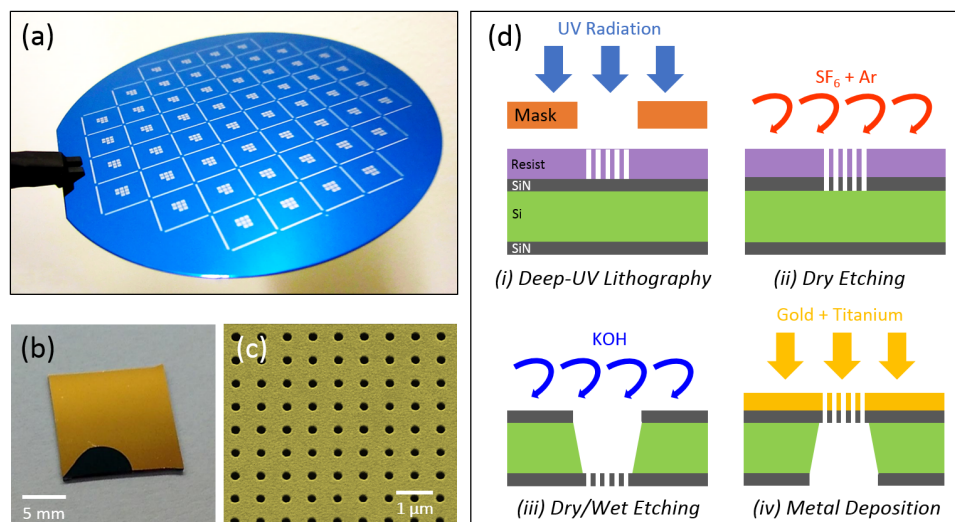
Figure 3 | Deep-UV Lithography based high-throughput fabrication of plasmonic nanohole arrays. (a) Photography of the wafer after deep-UV and dry etching steps. (b) Single plasmonic chip containing eight plasmonic pixels. (c) SEM image of the nanohole array with a hole diameter of 200 nm and an array period of 600 nm. (d) Fabrication steps of the nanohole arrays on free-standing silicon nitride membrane.

free detection approach, a minimum detectable IR of 1.31 (a.u.) (indicated by a red line in Fig. 4c) has been calculated by adding twice the standard deviation to the mean intensity ratio value of the reference sensor (response of the nanohole array under DI-water). This IR value (1.31) corresponds to a minimum detectable wavelength shift of 1.5 nm, denoted by a red line in Fig. 4b, which is equivalent to a minimum detectable refractive index change of $\sim 2 \times 10^{-3}$ RIU calculated using a refractive index sensitivity (RIS) of 621 nm/RIU (see the Methods section for refractive index sensitivity analysis using an optical spectrum analyzer). For the lensfree detection scheme that is based on diffraction pattern intensity changes, the minimum detectable relative intensity ratio is obtained as 0.01881, which corresponds to a minimum detectable refractive index change of $\sim 1 \times 10^{-3}$ RIU, calculated using a RIS of 17.53924/RIU (see the Methods section for our refractive index sensitivity analysis). These results suggest that the presented dual color biosensing platform that is integrated with microfluidics yields more than two fold improvement in the detection limit compared to our earlier single color lensfree detection design[12]. This sensitivity enhancement is attributed to our ratiometric analysis based on dual-wavelength illumination that digitally improves the detectable differences of refractive index changes occurring in the near-field of our plasmonic substrate.

In our biosensing device, as we utilize a microfluidic chip integrated with an imaging based platform, we can perform high-throughput analysis of protein-protein binding kinetics. Through a ratiometric digital analysis based on the dual-wavelength diffraction images, we can quantify the biomolecular interactions, revealing the real-time binding analysis of protein-protein complexes. For proof of concept demonstration, we utilize protein A/G and IgG antibody (see the Methods section for the details of our protein detection experiments), where we performed time lapse measurements within the microfluidic channels to detect their affinity as schematically illustrated in Fig. 5a. In Fig. 5, we demonstrate the association phase results for protein IgG (200 μg/mL) onto protein A/G (100 μg/mL) over 80 minutes of injection time. In this phase, the binding events of IgG to A/G result in an exponential increase in the peak wavelength shift as well as in the intensity ratio curve, leading to the saturation of our plasmonic sensor response since the binding sites on the plasmonic substrate is covered by the continuously injected protein IgG. Fig. 5c shows the dual-wavelength diffraction patterns of 3 different plasmonic pixels located on the same substrate, which are acquired simultaneously by our lensfree on-chip imager before (at time, t_0),

and after (at time, t_f) the binding events. This simultaneous detection capability of our biosensing platform is very important for high-throughput and multiplexed screening applications. Fig. 5d shows the variation in the intensity ratio of these diffraction image pairs over 80 minutes of association phase (see the Methods section for protein binding analysis). At each time point, three different sensor elements (separated by 1 mm) have very similar intensity responses and binding kinetics indicating that our hand-held device could operate uniformly over a large field-of-view. To validate our lensfree biosensing results, we also measure the peak wavelength of the plasmonic resonance before and after the IgG injection using an optical spectrum analyzer. Fig. 5d inset displays the amount of the spectral shift between injection start and stop times (80 minutes duration), providing ~ 6 nm peak wavelength shift for these 3 different plasmonic pixels (see Supplementary Fig. 4). It is important to note that the same target analyte that flows over different pixels yields the same wavelength shift and a comparable change in our lensfree intensity ratio, confirming robust detection of protein complexes using our platform.

The biomolecular interactions between the target protein IgG and the immobilized protein A/G can be modeled with the following differential equation[18].

$$d[IgG-A/G]/dt = k_a[IgG][A/G] - k_d[IgG-A/G] \qquad (1)$$

For the spectrum based biosensing measurements, the change rate of the peak wavelength shift, $d\Delta\lambda/dt$, is directly related to the formation of the protein complex $[IgG - A/G]$. Therefore, Equation 1 can be integrated to determine the association rate equation[18].

$$\Delta\lambda_t = k_a[IgG]\Delta\lambda_{max}\left(1 - e^{(-k_a[IgG]+k_d)t}\right)\Big/(k_a[IgG]+k_d) \qquad (2)$$

where $\Delta\lambda_{max}$ is the maximum peak wavelength shift when all the available binding sites are occupied and $\Delta\lambda_t$ is the peak wavelength shift from the initial peak wavelength at time t. This provides the relation between the peak wavelength shift of the plasmonic chip and the binding events as follows:

$$\Delta\lambda_t = \Delta\lambda_0\left(1 - e^{(-k_a[IgG]+k_d)t}\right) \qquad (3)$$

where $\Delta\lambda_0 = (k_a[IgG]\Delta\lambda_{max})/(k_a[IgG] + k_d)$.

Fig. 5b shows the amount of peak wavelength shift from its initial position (just before the IgG insertion) obtained by an optical spectrum analyzer in real-time from a single plasmonic pixel during the
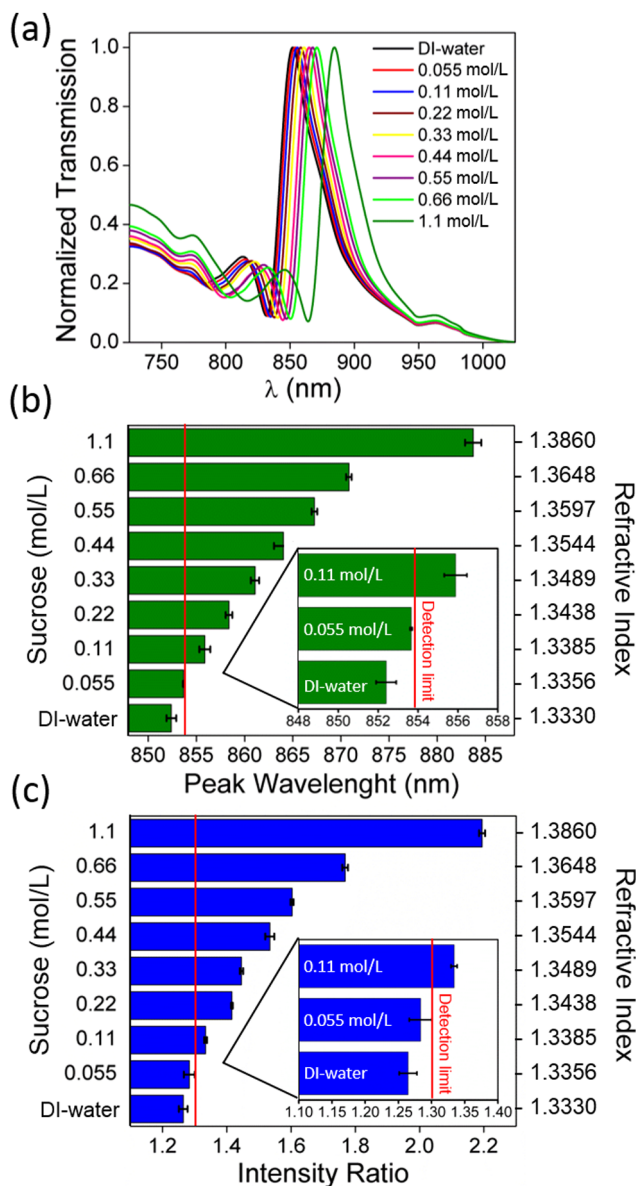
Figure 4 | Quantification of sucrose solutions at different concentrations and refractive indices using our computational plasmonic biosensing platform on a microfluidic chip. (a) Spectral response of the plasmonic sensors under various concentrations of sucrose samples, ranging from 0.055 to 1.1 mol/L. Analysis of (b) the peak wavelength shift in the plasmonic mode determined from the optical spectrometer measurements and (c) the corresponding intensity ratio analysis determined using the dual-wavelength lensfree images (error bar at each data point corresponds to the measurements obtained from 3 different samples). Figure inset: Zoomed version of the lower concentration sucrose measurements to demonstrate the detection limit, shown with a red line.

association phase of IgG. Based on the functional form presented in Equation 3, we perform an exponential fit on this experimental spectrum data, which provides:

$$\Delta\lambda = 6.448\left(1 - e^{-0.0005333t}\right) \quad (4)$$

Following the same strategy, for our lensfree on-chip biosensor, the change in the IR can be related to the amount of biomolecular events as follows:

$$IR_t = IR_0\left(1 - e^{(-k_a[IgG] + k_d)t}\right) \quad (5)$$

Thus, similar to Equation 4, we can obtain an exponential fit to our lensfree experimental data yielding:

$$IR = 0.10188\left(1 - e^{-0.0005685t}\right) \quad (6)$$

Equations 4 and 6 reveal that two independent experiments (one using an optical spectrum analyzer and the other using our dual-wavelength lensfree sensor) yield similar exponential constants, 0.0005333 and 0.0005685, respectively.

Methods

The presented biosensing platform relies on multiple hardware and software sub-components as detailed in the following subsections:

Fabrication of plasmonic substrates. Our fabrication process based on a deep-UV lithography method is illustrated in Fig. 3d. We start the fabrication process with a 500-μm-thick silicon wafer that is coated with 100 nm-thick nitride films on both sides. We first perform UV lithography to pattern the nanohole arrays with a Stepper (ASML S500/300 DUV). We then develop the photoresist and etch through the top silicon nitride layer to manufacture nanohole arrays using Plasma Therm 790 RIE/PECVD with SF_6 and Ar gases. We remove the remaining residues on the silicon nitride surface by oxygen plasma cleaning. Following that, we pattern a 750 μm × 750 μm window at the bottom silicon nitride layer through photolithography performed on 2 μm thick positive photoresist (Microposit™ S1818™) using a SUSS Mask Aligner (MicroTec MA/BA6). Following the development of the photoresist layer, we completely remove the silicon nitride layer within the transferred patterns at the backside of the wafer. We then immerse the chip in KOH solution in order to create freestanding silicon nitride membranes. We finally deposit Ti layer (adhesion layer, 5 nm thick) and Au layer (125 nm thick), providing plasmonic nanohole arrays without the need for a lift-off process. Each plasmonic biosensor pixel has a dimension of 100 μm × 100 μm, consisting of nanohole arrays each with a diameter of 200 nm and a period of 600 nm.

Assembly of microfluidic system. To build microfluidic channels over nanohole arrays, our plasmonic substrate is bonded to 4 layers of optically clear polyolefin film (~50 μm thick) that is patterned with a cutting plotter from Graphtec (see Supplementary Fig. 1). The assembled microfluidic chip has a channel height of ~100 μm and a flow chamber size of 4 mm × 4 mm, which is used to perform leak-free and low dead-volume flow experiments.

Sensitivity measurements. Test solutions are prepared by dissolving 0.3754 ± 0.0002 grams of sucrose (Molecular weight: 342.2 g/mol) in 1.00 mL volume of Deionized (DI) water, providing a 1.10 mol/L stock solution of sucrose 1.10 M. Such solution is then further diluted with DI water at different concentrations, ranging from 0.055 to 1.10 mol/L, corresponding to refractive indices of 1.3356 to 1.3860, measured with a refractometer (ATAGO PAL-series). These liquid samples are then used to evaluate the sensitivity of our biosensing platform.

Spectroscopic analysis. For biodetection experiments based on the peak wavelength shift of plasmonic modes, we mount our samples onto a Nikon Eclipse-Ti inverted microscope which is fiber coupled to an optical spectrometer (SpectraPro 500i spectrometer) and obtain the spectra under a normally incident white light illumination.

Protein detection experiments. Initially, a 100 μg/mL protein A/G solution (recombinant fusion protein with protein A and protein G binding sites dissolved in phosphate buffered saline (PBS) 1×, pH 7.4) is incubated on a freshly cleaned plasmonic substrate for 20 minutes. Following the PBS wash of the chip 3 times, the substrate is rinsed with DI water and dried with Nitrogen. A thin layer (~3 nm) of protein A/G forms on the gold surface by physisorption[12]. This substrate is then integrated with the microfluidic system, followed by the injection of a PBS solution through the channel. Once the plasmonic sensor response is stabilized, we inject Human IgG protein with an injection rate of ~10 μL/minute for 80 minutes, achieving ~12.5 picomoles per minute (Molecular Weight: 160 kDa, Concentration: 200 μg/mL), exhibiting an association phase of IgG onto the A/G proteins. Finally, PBS is injected, which removes the excess IgG proteins that do not bind to the A/G proteins. As a result of this association phase, an ~8 nm thick bilayer of protein A/G and antibody IgG complex is formed on the gold surface, and the binding events are detected in real-time by our on-chip sensing platform. During the binding of IgG antibody with the A/G proteins, the number of IgG molecules increases within the ~8 nm thick film. At the end of the experiment, when the available binding sites are occupied by the IgG antibody, the optical response of the plasmonic sensor saturates.

Binding analysis of protein-protein interactions. Binding kinetics analysis of protein A/G and IgG can be summarized in two sequential steps: (i) In the association phase, IgG antibody protein is flowed over the sensor surface that is already functionalized with protein A/G, creating a protein complex, $IgG + A/G \rightarrow [IgG - A/G]$. This binding process depends on the association constant ($k_a \sim 3.110x$ $10^5 \, M^{-1}s^{-1}$) that demonstrates the predisposition of the small molecules to form larger composites. (ii) In the dissociation phase, only a buffer is flowed over the
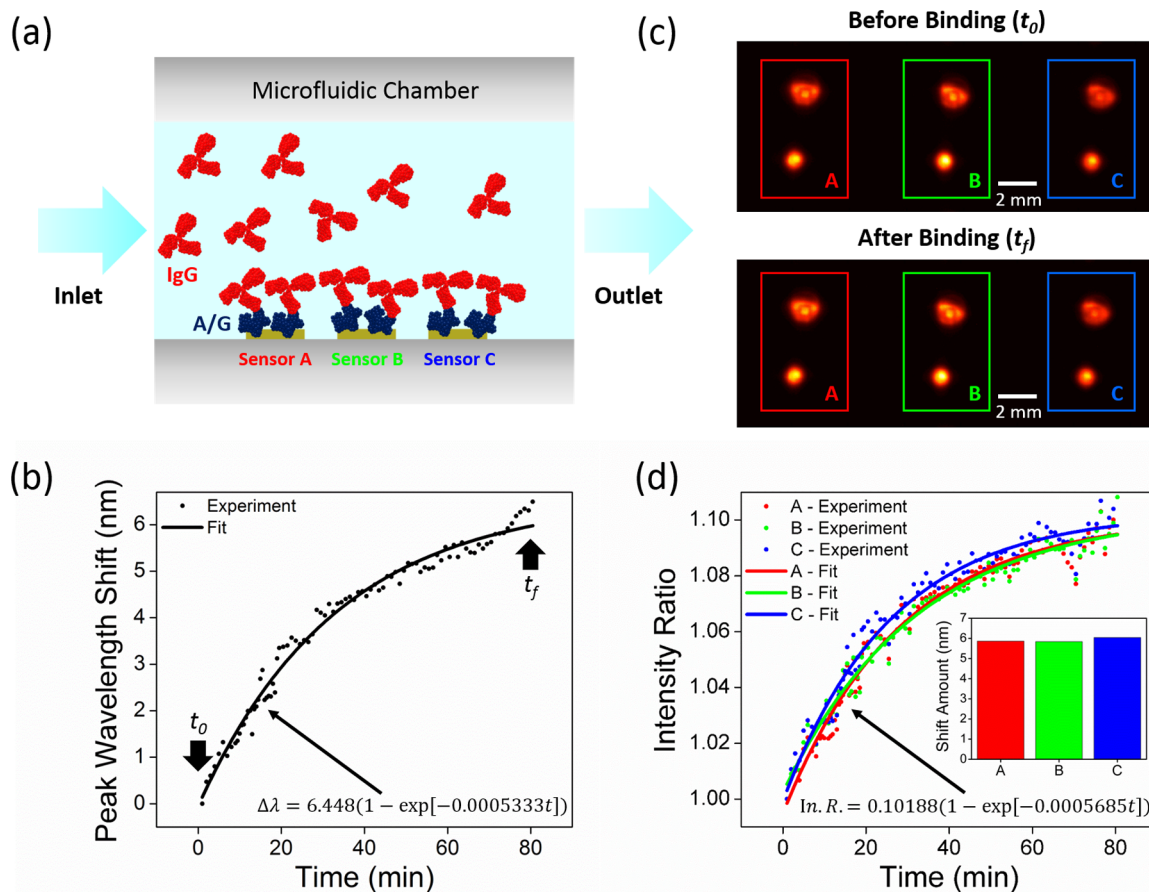
Figure 5 | Monitoring of binding kinetics of protein/protein interactions. (a) Schematic illustration of IgG and A/G protein interactions on the plasmonic chip, containing 3 sensors (A, B, C), integrated with a microfluidic chamber. (b) Exponential fit to the real-time measurement results obtained by an optical spectrum analyzer. (c) Lensfree diffraction patterns of the nanohole arrays formed by dual LED illumination before (t_o) and after (t_f) the binding of the protein IgG on the surface of the plasmonic chip containing 3 sensors, covered with protein A/G. (d) Exponential fit to our lensfree dual-wavelength measurement results. Figure inset: The validation of lensfree biosensing through optical spectrometer measurements performed before and after the IgG binding, providing the same amount of peak wavelength shift (~6 nm) for 3 different plasmonic sensors.

surface, where the protein complex on the surface is detached to give free individual proteins, i.e., $[IgG - A/G] \rightarrow IgG + A/G$. This removal process depends on the disassociation constant ($k_d < 10x\ 10^{-6}\ s^{-1}$) that measures the affinity of larger objects to separate reversibly into smaller components. The dissociation constant for Protein A/G and Human IgG antibody is $k_d < 10x\ 10^{-6}\ s^{-1}$ [19], indicating that the composite is highly stable once it is formed and a minimum amount of IgG will remain unbound. These binding events are monitored through our lensfree plasmonic sensing platform and used to further analyze protein-protein interactions, e.g., kinetics and thermodynamic parameters and concentration, as commonly performed in SPR literature[19].

Dual-color lensfree imaging set-up. In order to record the diffraction patterns of plasmonic pixels, we designed a lensfree imaging platform using a CMOS imager (IDS, model: UI-1481LE, 5 Megapixel with 2.2 μm pixel size), two LEDs (Digikey, models: 1125-1088-ND and 751-1211-ND, 820 and 880 peak wavelengths, 28 nm and 40 nm bandwidth, respectively) that are positioned at $D = 11\ mm$ lateral spacing, and one button battery (3V Lithium Renata CR 2032). These parts are then inserted into a mechanical housing that is designed in Inventor (Autodesk) and manufactured using a 3D printer (Elite, Dimension). In this imaging geometry, LED source to plasmonic chip ($h_1 \sim 6.7\ cm$) and substrate to sensor array distance ($h_2 \sim 3\ mm$) determine the center-to-center distance between the dual diffraction patterns (d). In this current device, the center-to-center LED separation distance, $D = 11\ mm$ provides a diffraction pattern separation of $d = 0.5\ mm$ based on the ratio of h_1/h_2 (see Supplementary Fig. 2 for various d and D combinations). Once the plasmonic chip is inserted into our portable device, the constituting components are mechanically aligned in the compact unit for subsequent biosensing experiments.

Digital processing of lensfree diffraction images. We start the digital analysis of lensfree images by spatially localizing the centroids of dual-wavelength diffraction patterns. In these images, dual diffraction patterns for each plasmonic pixel are determined by assigning two neighboring regions of interest (ROIs) to a single plasmonic pixel. The total transmission signal for each ROI is then calculated by

summing up the pixel photon count values over an area of 200 × 200 pixels. Based on this calculation, for each dual-wavelength diffraction pattern, the total transmission signal of the ROI illuminated by 880 nm LED (I_{880}) is divided by the signal of the ROI illuminated by 820 nm LED (I_{820}) to calculate an IR per plasmonic pixel:

$$IR = I_{880}/I_{820}$$

These measured IR values are used to quantify the binding events occurring in the vicinity of the plasmonic chip (see e.g., Equation 6). For a series of lensfree frames, the same ROIs are used for every plasmonic pixel on the substrate, where the IR values were plotted against the number of frames to monitor the protein-protein binding interactions over time. In this proof-of-principle demonstration, the intensities of the two LEDs were not the same. The one at 820 nm is brighter than the one at 880 nm, which results in an intensity difference between the two diffraction patterns detected by the CMOS imager (Fig. 2b). Our ratiometric analysis eliminates the contributions from such mismatches between the two LEDs.

Refractive index sensitivity (RIS) analysis. RIS is used to calculate the refractive index change of the surrounding medium based on the ratio of the change in the resonance wavelength of the plasmonic mode to the change in the refractive index of the medium ($RIS = \Delta\lambda/\Delta n$). For the nanohole array used in this work, we measure the transmission signals of the bare nanohole array ($\lambda_{resonance,air} = 647\ nm$) and the nanohole array embedded in DI-water ($\lambda_{resonance,water} = 852\ nm$), providing a resonance shift of 205 nm. This results in an RIS value of 621 nm/RIU. For spectrometer based measurements, Δn of target samples can then be calculated by dividing $\Delta\lambda$ to the RIS value, which is $\Delta n = \Delta\lambda/RIS$.

For our lensfree sensing approach, RIS is defined as the ratio of the change in the diffraction pattern intensity to the change in the refractive index of the medium, i.e., $RIS = \Delta IR/\Delta n$. In our platform, we obtain the intensity ratio for the nanostructures measured in DI-water ($IR_{Water} = 1.26468$) and in 1.1 mol/L sucrose solution ($IR_{Sucrose} = 2.19426$), yielding an intensity ratio change of 0.92958. This provides an RIS value of 17.53924/RIU. Δn of the target samples can then be calculated by dividing ΔIR to the RIS value, i.e., $\Delta n = \Delta IR/RIS$.

Conclusion

We demonstrated a microfluidics based biosensing platform that combines large-scale plasmonic microarrays with dual-wavelength lensfree on-chip imaging for multiplexed and label-free monitoring of binding events over a large field-of-view. This integrated biosensing platform, weighing 40 grams with 8.8 cm in height, utilizes a CMOS imager to record the diffraction patterns of plasmonic nanoapertures located at the bottom of a micro-channel under simultaneous illumination by two different color LEDs located spectrally at the right and left sides of the plasmonic mode. In this approach, variations in the refractive index of the medium surrounding the plasmonic nanohole arrays shifts the plasmonic mode of these nanostructures, which enhances the transmission signal of one of the diffraction patterns and decreases the transmission signal of the other one. These acquired images are then processed through the use of a ratiometric digital analysis method. Using the presented plasmonic biosensor, we successfully monitored the real-time binding kinetics of protein A/G and protein IgG interactions. We also introduced a deep UV lithography based fabrication method, rapidly creating thousands of plasmonic nanostructures at low cost. This provides a timely solution to the fabrication challenge of large-scale plasmonic arrays that can be simultaneously screened with large field-of-view imaging systems. Our plasmonic biosensing platform would be highly advantageous for real-time and high-throughput analysis of biomolecular interactions at resource-poor settings.

1. Zhu, H., Isikman, S. O., Mudanyali, O., Greenbaum, A. & Ozcan, A. Optical imaging techniques for point-of-care diagnostics. *Lab. Chip* **13**, 51–67 (2013).
2. Zhu, H., Sikora, U. & Ozcan, A. Quantum dot enabled detection of Escherichia coli using a cell-phone. *The Analyst* **137**, 2541–2544 (2012).
3. Coskun, A. F. et al. A personalized food allergen testing platform on a cellphone. *Lab. Chip* **13**, 636–640 (2013).
4. Coskun, A. F., Nagi, R., Sadeghi, K., Phillips, S. & Ozcan, A. Albumin testing in urine using a smart-phone. *Lab. Chip* **13**, 4231–4238 (2013).
5. Cooper, M. A. Label-free screening of bio-molecular interactions. *Anal. Bioanal. Chem.* **377**, 834–842 (2003).
6. Zhang, Y. et al. Towards a high-throughput label-free detection system combining localized-surface plasmon resonance and microfluidics. *Lab. Chip* **12**, 3012–3015 (2012).
7. Choi, C. J. & Cunningham, B. T. A 96-well microplate incorporating a replica molded microfluidic network integrated with photonic crystal biosensors for high throughput kinetic biomolecular interaction analysis. *Lab. Chip* **7**, 550–556 (2007).
8. White, I. M., Oveys, H., Fan, X., Smith, T. L. & Zhang, J. Integrated multiplexed biosensors based on liquid core optical ring resonators and antiresonant reflecting optical waveguides. *Appl. Phys. Lett.* **89**, 191106 (2006).
9. Daaboul, G. G. et al. LED-based Interferometric Reflectance Imaging Sensor for quantitative dynamic monitoring of biomolecular interactions. *Biosens. Bioelectron.* **26**, 2221–2227 (2011).
10. Chang, T.-Y. et al. Large-scale plasmonic microarrays for label-free high-throughput screening. *Lab. Chip* **11**, 3596–3602 (2011).
11. Brolo, A. G. Plasmonics for future biosensors. *Nat. Photonics* **6**, 709–713 (2012).
12. Cetin, A. E. et al. Handheld high-throughput plasmonic biosensor using computational on-chip imaging. *Light Sci. Appl.* **3**, e122 (2014).
13. Ebbesen, T. W., Lezec, H. J., Ghaemi, H. F., Thio, T. & Wolff, P. A. Extraordinary optical transmission through sub-wavelength hole arrays. *Nature* **391**, 667–669 (1998).
14. Yanik, A. A. et al. Seeing protein monolayers with naked eye through plasmonic Fano resonances. *Proc. Natl. Acad. Sci.* **108**, 11784–11789 (2011).
15. Yanik, A. A. et al. An Optofluidic Nanoplasmonic Biosensor for Direct Detection of Live Viruses from Biological Media. *Nano Lett.* **10**, 4962–4969 (2010).
16. Khademhosseinieh, B. et al. Lensfree sensing on a microfluidic chip using plasmonic nanoapertures. *Appl. Phys. Lett.* **97** (2010).
17. Kim, J. Joining plasmonics with microfluidics: from convenience to inevitability. *Lab. Chip* **12**, 3611–3623 (2012).
18. Saha, K., Bender, F. & Gizeli, E. Comparative Study of IgG Binding to Proteins G and A: Nonequilibrium Kinetic and Binding Constant Determination with the Acoustic Waveguide Device. *Anal. Chem.* **75**, 835–842 (2003).
19. Bronner, V. T. et al. Rapid Screening and Selection of Optimal Antibody Capturing Agents Using the ProteOn XPR36 Protein Interaction Array System. *Bio-Rad Technical Note* **5820** (2006).

Author contributions

A.F.C., A.E.C. and B.C.G. conducted the experiments and analyzed the resulting data. D.A.A. contributed to experiments and methods. A.F.C., A.E.C., B.C.G., H.A. and A.O. wrote the manuscript. A.O. and H.A. supervised the project.

Additional information

Supplementary information accompanies this paper at http://www.nature.com/scientificreports

Competing financial interests: A.O. is the co-founder of a start-up company (Holomic LLC) which aims to commercialize computational imaging and sensing technologies licensed from UCLA.

How to cite this article: Coskun, A.F. et al. Lensfree optofluidic plasmonic sensor for real-time and label-free monitoring of molecular binding events over a wide field-of-view. *Sci. Rep.* **4**, 6789; DOI:10.1038/srep06789 (2014).